This is the accepted manuscript made available via CHORUS. The article has been published as:

Measurements of ion-electron energy-transfer cross section in high-energy-density plasmas

P. J. Adrian, R. Florido, P. E. Grabowski, R. Mancini, B. Bachmann, L. X. Benedict, M. Gatu Johnson, N. Kabadi, B. Lahmann, C. K. Li, R. D. Petrasso, H. G. Rinderknecht, S. P. Regan, F. H. Séguin, R. L. Singleton, Jr., H. Sio, G. D. Sutcliffe, H. D. Whitley, and J. A. Frenje

Phys. Rev. E **106**, L053201 — Published 8 November 2022

DOI: 10.1103/PhysRevE.106.L053201

Measurements of ion-electron energy-transfer cross section in High Energy Density Plasmas

P. J. Adrian,[1] R. Florido,[2] P. E. Grabowski,[3] R. Mancini,[4] B. Bachmann,[3] L. X. Benedict,[3] M. Gatu Johnson,[1] N. Kabadi,[1] B. Lahmann,[1] C. K. Li,[1] R. D. Petrasso,[1] H. G. Rinderknecht,[5] S. P. Regan,[5] F. H. Séguin,[1] R. L. Singleton Jr.,[6,7] H. Sio,[3] G. D. Sutcliffe,[1] H. D. Whitley,[3] and J. A. Frenje[1]

[1]*Plasma Science and Fusion Center, Massachusetts Institute of Technology, Cambridge, Massachusetts 02139, USA*
[2]*iUNAT - Departamento de Fsica, Universidad de Las Palmas de Gran Canaria, 35017 Las Palmas de Gran Canaria, Spain*
[3]*Lawrence Livermore National Laboratory, Livermore, California 94550, USA*
[4]*Physics Department, University of Nevada, Reno, Nevada 89557, USA*
[5]*Laboratory for Laser Energetics, University of Rochester, Rochester, New York 14623, USA*
[6]*SavantX Research Center, Santa Fe NM, 87501, USA*
[7]*School of Mathematica, University of Leeds, Leeds, United Kingdom*

(Dated: September 1, 2022)

We report on the first measurements of the ion-electron energy-transfer cross section utilizing low-velocity ion-stopping in High Energy Density plasmas at the OMEGA laser facility. These measurements utilize a new and unique technique that leverages the close relationship between low-velocity ion stopping and ion-electron equilibration. Shock-driven implosions of capsules filled with D^3He gas doped with a trace amount of Argon were used to generate densities and temperatures in the range of $1 \times 10^{23} \rightarrow 2 \times 10^{24}$ cm^{-3} and $1.4 \rightarrow 2.5$ keV, respectively. The energy loss of 1-MeV DD-tritons and 3.7-MeV D^3He-alphas that had velocities lower than the average velocity of the thermal electrons were measured. The energy loss of these ions were used to determine the ion-electron energy-transfer cross section which was found to be in excellent agreement with quantum mechanical calculations in the first-Born approximation. This result provides the first experimental constraint on ion-electron energy transfer in High Energy Density plasmas, which impacts the modeling of alpha heating in inertial confinement fusion implosions, magnetic field advection in stellar atmospheres, and energy balance in supernovae shocks.

Obtaining a fundamental understanding of ion-electron (i-e) energy transfer is an essential prerequisite for correctly describing the evolution of High Energy Density (HED) and Inertial Confinement Fusion (ICF) plasmas. This is especially important in scenarios where ions and electrons are differentially heated and the i-e collision frequency is on the order of the plasma-evolution time scale. Scenarios where i-e collisions play an important role are: shock waves where i-e collisions dictate the plasma profiles [1], laser ablation where electron heating is driven by inverse-Bremsstrahlung [2], magnetic-field advection where fields are reorganized by the Nernst effect [3], alpha heating in ICF implosions where i-e collisions mediate the nuclear-burn wave [5–7], the core-collapse of supernovae where ion-electron collisions impact the magnetic Raleigh-Taylor instability [4], and shocks in supernova remnants [8–10]. To understand the dynamics of these plasmas, models and theories of i-e collisions must be accurate over a wide range of plasma conditions. While extensive theoretical work has been done to describe i-e collisions [11–32], there is a paucity of experimental methodologies to test these theories. The lack of data prevents model validation and increases the level of uncertainty in simulations of HED plasmas [33]. To our knowledge, only, two experiments have made an attempt to study i-e energy-transfer at high density ($> 10^{23}/cm^3$) and temperature (> 1 keV) in implosions [34, 35]. However, the implosion dynamics [34], 3D asymmetries [36] and thermal gradients [37] severely complicated their interpretation of the time-integrated results.

In this letter, we report on the first precision measurements of the i-e energy-transfer cross section in HED plasmas using a novel measurement technique that avoids the complications in previous work. The new experimental methodology utilizes the stopping power of nearly mono-energetic ions below the Bragg peak for the determination of the Coulomb logarithm (proportional to the i-e energy-transfer cross section) for electron densities (n_e) and temperatures (T_e) in the range of $1 \times 10^{23} \rightarrow 2 \times 10^{24}$ cm^{-3} and $1.4 \rightarrow 2.5$ keV.

I-e equilibration depends on the i-e energy-transfer cross section of thermal ions scattering off thermal electrons, while ion stopping power depends on the momentum-transfer cross section of arbitrarily fast ions interacting with the thermal electrons. When the velocity of the projectile ions (V_i) is lower than the average velocity of the thermal electrons (V_{Te}), i.e $V_i < V_{Te}$, the cross sections for energy and momentum transfer are trivially related. In fact it has been shown previously [14, 16, 17, 28, 39] that

TABLE I. Experimental implosion parameters and key plasma conditions for inferring an experimental Coulomb logarithm, $\ln\Lambda_{exp}$

Shot	Fill $D_2/^3He/Ar$ [atm]	Laser[69] [kJ]	Bang Times [63] [ps] DD	D^3He	X-ray	Yields [64] DD	D^3He	Temp. [keV] $\langle T_i\rangle$ [66]	$\langle T_e\rangle$ [67]	$\langle n_e\rangle^f$ [$\times10^{23}$cm^{-3}]	$\langle n_eL\rangle^f$ [$\times10^{21}$cm^{-2}]	$\Delta E_i/Z_i^2$ [MeV] [65] DD-t [68]	D^3He-α	$\ln\Lambda_{exp}$
78608	5.0/11.3/0.10	7.4	1190	1220	–	2.0×10^9	1.4×10^9	5.9±0.3	1.4±0.1	21±4.2	5.0±1.0	0.28	0.47	2.9±0.8
78609	5.0/11.7/0.11	7.2	1217	1240	–	1.6×10^9	1.1×10^9	5.6±0.3	1.4±0.1	21±4.2	5.0±1.0	0.35	0.51	3.4±1.1
78611	5.0/11.3/0.10	6.4	1327	1360	–	5.4×10^8	6.3×10^8	4.8±0.3	1.6±0.2	11±4.5	4.5±0.9	–	0.42	4.1±1.1
78612	5.0/11.5/0.12	6.1	1309	1334	–	6.2×10^8	5.2×10^8	5.0±0.3	1.6±0.2	11±4.5	4.5±0.9	–	0.42	4.0±1.1
75694	3.0/6.8/0.15	12.0	1065	1100	1140	1.5×10^{10}	1.1×10^{10}	8.8±0.3	2.8±0.3	6.6±1.0	4.1±0.4	0.19	0.28	5.8±1.4
75695	3.0/6.7/0.14	9.9	1095	1163	1215	1.1×10^{10}	5.9×10^9	7.8±0.3	2.3±0.2	4.6±0.7	4.5±0.5	0.30	0.41	5.1±1.5
75698	3.0/6.0/0.14	9.9	1110	1173	1220	1.1×10^{10}	5.3×10^9	7.6±0.3	2.1±0.2	4.8±0.7	4.3±0.4	0.25	0.41	5.3±1.4
75699	3.0/6.7/0.12	8.1	1195	1254	1292	7.3×10^9	2.3×10^9	6.6±0.3	1.9±0.2	3.9±0.6	3.9±0.4	0.28	0.41	5.4±1.5
75700	3.0/6.7/0.12	8.0	1185	1258	1300	6.6×10^9	2.1×10^9	7.0±0.3	1.9±0.2	3.8±0.6	4.2±0.4	0.24	0.34	4.4±1.2
75701	3.0/6.5/0.15	6.6	1330	1360	1430	2.7×10^9	3.2×10^8	4.6±0.3	1.8±0.2	5.1±0.8	3.2±0.3	0.34	0.45	4.2±1.2
75702	3.0/7.1/0.14	6.3	1350	1398	1525	2.4×10^9	2.7×10^8	4.5±0.3	1.4±0.2	3.8±0.8	5.2±0.3	0.27	0.40	3.9±1.1

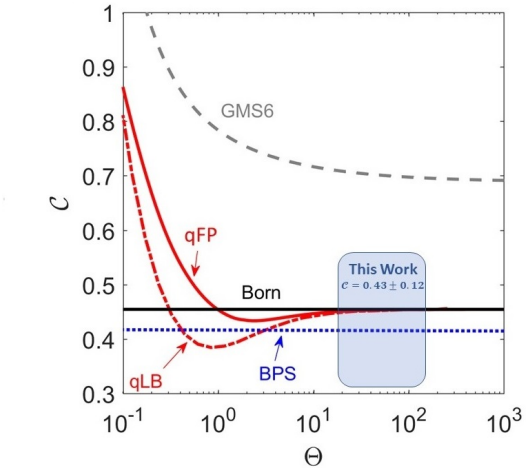


FIG. 1. Parameter $\mathcal{C}$ as a function of Θ for qLB (red dash-dotted), qFP (red solid), BPS (blue dotted), and GMS6 (gray dashed) theories evaluated at the $T_e = 2$ keV and $Z_i = 1$. Also shown is $\mathcal{C}$ computed in the first Born-approximation (black solid). As discussed in the text, this work probed Θ = 20-100, where $\mathcal{C}$ is insensitive to the plasma conditions and thus has a very weak dependence on Z_i. The blue box represents the constraints on $\mathcal{C}$ obtained from measurements detailed in this work. Evaluations of the Coulomb logarithm for each theory are found in the Supplemental Information.

for $V_i < V_{Te}$ the ion stopping is expressed as

$$\frac{dE}{dx} = -\nu_{ie}^p m_i V_i(x), \tag{1}$$

where m_i is the mass of the ion and ν_{ie}^p is the momentum transfer frequency given by

$$\nu_{ie}^p = \frac{4\pi}{3}\sqrt{\frac{2}{\pi}}\sqrt{\frac{m_e}{m_i^2}}Z_i^2 e^4 \frac{n_e}{T_e^{3/2}}\ln\Lambda, \tag{2}$$

for a weakly coupled and non-degenerate plasma (CGS units). Here, $\ln\Lambda$ is the Coulomb logarithm, m_e is the electron mass, and Z_i is the ion charge. Similarly, the temperature relaxation can be expressed as

$$\frac{dT_i}{dt} = -\nu_{ie}^E(T_i - T_e), \tag{3}$$

where T_i is the ion temperature and ν_{ie}^E is the energy transfer frequency. The energy and momentum transfer frequencies are related as $\nu_{ie}^E = 2\nu_{ie}^p$.

A tracer particle moving with $V_i < V_{Te}$ loses energy by an amount [61]

$$\Delta E_i = m_i V_i \langle\nu_{ie}^p\rangle - \frac{1}{2}m_i\langle\nu_{ie}^p\rangle^2, \tag{4}$$

where $\langle\nu_{ie}^p\rangle = \int \nu_{ie}^p dx$ is the path-integrated collision frequency. Thus, the energy-transfer cross section (or $\ln\Lambda$) governing both low-velocity stopping

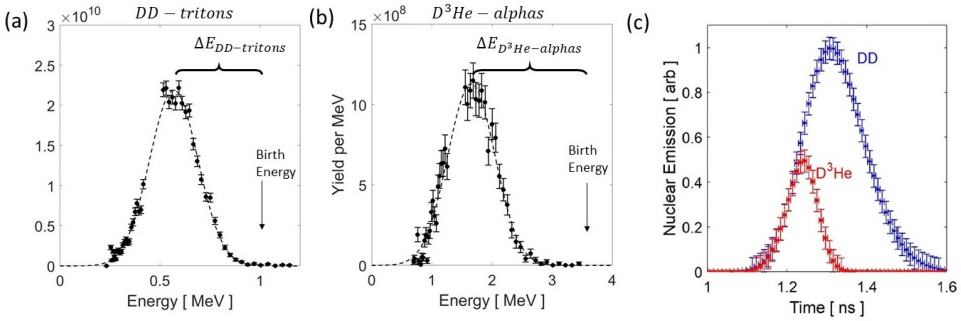


FIG. 2. An example of measured (a) DD-triton and (b) D^3He-alpha spectra (shot 78609). The birth energy and ΔE are indicated. (c) Measured DD and D^3He nuclear-reaction histories.

power and the ion-electron equilibration process is determined from measurements of ΔE_i, n_e, and T_e.

The connection between ion-stopping power and i-e equilibration has been exploited theoretically. First, the T-matrix formalism for calculating the collision term in Gericke's treatment of stopping power [40] was borrowed to calculate temperature relaxation [14]. Second, Bernstein *et. al.* [41] utilized this connection to investigate the effects of strong coupling on temperature relaxation through MD simulations. This work is the first experimental effort to utilize this connection.

The classical description of i-e energy transfer was first described by Landau and Spitzer (LS) [11, 12]. In the LS formalism, a Coulomb logarithm is included to regularize the integration of the i-e differential cross section for elastic scattering, which diverges due to improper treatment of the Coulomb potential. The Coulomb logarithm for a classical plasma is $\ln(\mathcal{C}_{CL}\lambda_{De}/\lambda_L)$, where $\lambda_{De} = \sqrt{T_e/4\pi n_e e^2}$ is the Debye length, $\lambda_L = Z_i e^2/T_e$ is the Landau length, $\mathcal{C}_{CL}$ is a correction factor derived from the weak-scattering approximation [22]. On the basis of calculations and simulations, $\mathcal{C}_{CL} = 0.765$ for classical plasmas [16, 18, 38]. This expression captures the screening physics at large impact parameters and local field corrections at the classical distance of closest approach. The LS theory breaks down because quantum diffraction, electron degeneracy and strong coupling are not considered. In recent years, various theories and computational tools have been developed to address the impact of quantum effects. The Gericke-Murillo-Schlanges (GMS) theory [14] is derived by using a quantum Boltzmann collision operator combined with a T-matrix calculation of the differential cross section for elastic scattering. This theory, which is widely used in radiation-hydrodynamics codes for modeling of ICF and HED plasmas, captures strong coupling and quantum-diffraction effects in the scattering process, but neglects aspects of the dynamical screening of the i-e interaction. This paper uses the 'GMS6' result which is a fit to the full T-matrix result and is the sixth entry in Table I of Ref [14]. The quantum Lenard-Balescu formalism (qLB) was developed for weakly-coupled plasmas to treat i-e interactions with a linear-response formalism [15, 22, 25, 26, 28, 31]. The qLB theory includes dynamical screening through a wave-vector and frequency dependent dielectric function evaluated in the Random-Phase Approximation (RPA) and considers Pauli blocking and quantum diffraction [23]. This theory has an analytic expression for calculating the i-e energy transfer cross section derived in Ref [31]. The quantum Landau/Fokker-Planck (qFP) theory [28] is the qLB result but ignores dynamic screening in the RPA dielectric response function. Brown, Preston, and Singleton (BPS) used dimensional-continuation to regularize the divergence in the integral of the i-e energy transfer cross section [16, 17]. This theory includes the modeling of quantum diffraction and electron degeneracy. Lastly, an analytical expression for the i-e cross section was computed using the first-Born approximation to calculate the scattering amplitudes of electrons interacting with a Debye screened potential [60]. All five theories have been implemented in various hydrodynamics codes to simulate HED plasmas [56, 57].

Central to this discussion is that the GMS, qLB, qFP, and BPS theories differ in the computation of the ion-electron Coulomb logarithm (i-e energy transfer cross section). Figure 1 illustrates the differences by fitting each theory to the form of $\ln\Lambda$ as $\ln(\mathcal{C}\lambda_{De}/\lambda_Q)$, where $\lambda_Q = \sqrt{\hbar^2/8m_eT_e}$ is proportional to the de Broglie wavelength, and $\mathcal{C}$ is a correction factor. Figure 1 displays $\mathcal{C}$ as a function of the degeneracy parameter, Θ, which is the ratio of T_e to the Fermi energy. For the various theories, $\mathcal{C}$ is independent of plasma conditions at the conditions

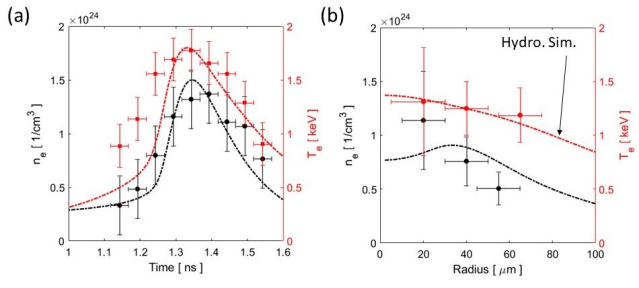


FIG. 3. An example of measured (data points) and hydro simulated (dash-dot) plasma conditions for shot 78609. (a) $n_e(t)$ and $T_e(t)$, (b) $T_e(r)$ and $n_e(r)$. Hydro-simulated plasma conditions were scaled with a constant multiplier.

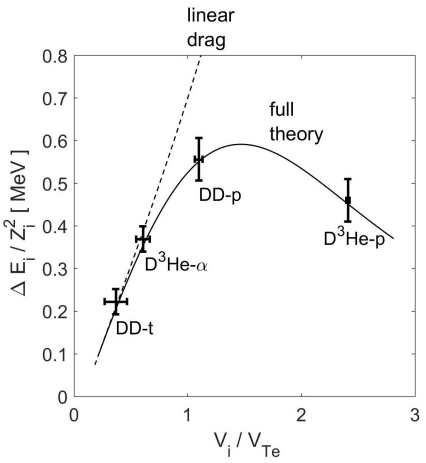


FIG. 4. An example of measured ΔE (normalized by Z_i^2) versus ion velocity, V_i, normalized by electron thermal velocity, V_{Te} (shot 78209). Black solid curve is the energy loss predicted by BPS theory for the plasma conditions given in Table I. The black dashed line represents the energy loss determined from the linear drag model when $V_i < V_{Te}$ [see Eq. 4].

relevant to this work, with GMS predicting $\mathcal{C} = 0.7$, and the qLB and qFP predict 0.45. Also shown in Figure 1 is the line $\mathcal{C} = 0.45$ which is predicted by the first-Born approximation (black solid) [60]. The BPS theory has a weak dependence on the electron temperature, T_e. The qLB, qFP, and BPS theories asymptote to the first-Born approximation at high Θ and T_e.

This work utilized the established methodology for precision ion-stopping-power measurements [42, 43] at the OMEGA laser facility [44]. Thin-shell glass capsules filled with D^3He and trace amounts of Argon gas were imploded. The capsule initial conditions and the laser parameters are summarized in Table I. The laser intensity on the capsule was kept

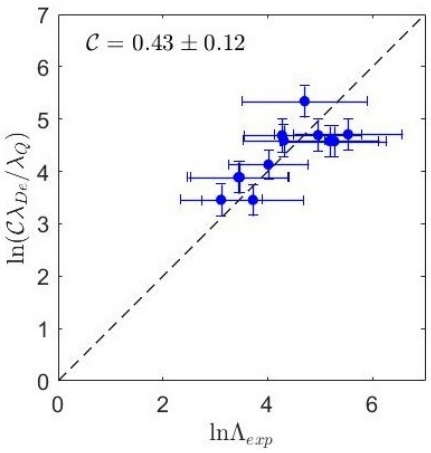


FIG. 5. The Coulomb logarithm $\ln(\mathcal{C}\lambda_{De}/\lambda_Q)$ versus measured $\ln\Lambda_{exp}$. The measurements of $\langle n_e \rangle$ and $\langle T_e \rangle$ were used to calculate λ_{De} and λ_Q. The value of $\mathcal{C}$, which minimizes $\ln\Lambda_{exp} - \ln(\mathcal{C}\lambda_{De}/\lambda_Q)$, was determined to be 0.43 ± 0.12.

below the two-plasmon-decay threshold to avoid capsule charging that would affect these measurements [45, 46]. As the laser ablates the glass shell, it drives a strong shock through the D^3He gas, which rebounds at the center of the implosion causing DD and D^3He fusion reactions. These reactions generate 1-MeV DD-tritons (t), 3.7-MeV D^3He-alphas (α), 3.0-MeV DD-protons (p) and 14.7-MeV D^3He-p. As the velocity of the DD-t ($\sim 5 \times 10^6$ m/s) and D^3He-α ($\sim 9 \times 10^6$ m/s) are below V_{Te} ($\sim 1.8 \times 10^7$ m/s at $T_e = 2$ keV) in these experiments, these low-velocity ions were used to probe i-e energy transfer cross section. Four measurements essential to this effort were (1) measurements of the DD- and D^3He- fusion-product spectra, (2) measurements of the DD and D^3He reaction histories, and (3-4) measurements of T_e(r,t) and n_e(r,t). The fusion-product spectra were measured with the Charged Particle Spectrometers (CPS) [47]. The energy loss, ΔE, of each fusion product was determined by subtracting the measured mean energy from the birth energy predicted by Ballabio *et al.* [48] using the measured average ion temperature, $\langle T_i \rangle$, shown in Table I. An example of measured DD-t and D^3He-α spectra and associated ΔE are shown in Fig 2(a) and (b). The measured $\Delta E_i/Z_i^2$ for the DD-t and D^3He-α are given in Table I.

The DD and D^3He reaction histories were measured simultaneously with the Particle X-ray Temporal Diagnostic (PXTD) [49] and an example of resulting data is show in Fig. 2(c). There is a systematic timing difference between the DD and D^3He reaction histories for all shots presented in this paper, indicating that the DD-t and D^3He-α sample differ-

ent plasma conditions. This data together with simulations are used to account for the effect of evolving plasma conditions that have an impact on the measured ΔE, as previously noted by Frenje *et al.* [43]. The DD and D^3He emission profiles were imaged using the Particle Core Imaging System [54].

Argon He-β, Ly-β, and Ly-γ line emissions were measured using a time-resolving x-ray spectrometer to infer used to infer $n_e(t)$ and $T_e(t)$ [50, 51]. Example data is shown in Fig. 3(a). These data clearly demonstrates that n_e increases about 20% from peak D^3He emission to peak DD emission, information that is necessary when correcting the measured ΔE of the D^3He-α.

Absolute $n_e(r)$ and $T_e(r)$ profiles were diagnosed with the Multi-Monochromatic Imager (MMI) through measurements of the spatial distribution of Argon line emission [52]. Example profiles are shown in Fig. 3(b). These profiles, which were integrated over a time gate of 100 ps during the x-ray emission period, were used to scale the magnitude of the HYADES [53] simulated profiles. The comparison between the measured and simulated profiles for shot 78609 is also shown in Fig. 3(b).

A one-dimensional code was developed and used to transport the DD-t and D^3He-α through the well-characterized evolving density and temperature profiles. In the code, the source characteristics of these two fusion products were determined from the PCIS and PXTD data. At each step (in time and space) the fusion products felt the local friction computed from the Maynard-Deutsch stopping-power model [58, 59]. The fractional energy lost was also computed and was used to compute the dE/dx-weighted plasma conditions $\langle T_e \rangle$, $\langle n_e \rangle$, and $\langle n_e L \rangle$ at each step (for more information see Supplemental Information). These parameters are presented in Table I for every shot. The quantities represent the average conditions that particles probe accounting for the evolving plasma conditions.

The $\langle T_e \rangle$ and $\langle n_e \rangle$ values were used to generate BPS-predicted $\Delta E_i/Z_i^2$ curves versus V_i/V_{Te} that are contrasted to the measured data for all four fusion products shown in Figure 4. The comparison clearly indicates that the BPS theory does an excellent job describing the measured energy loss [62] as already demonstrated in Ref. [43]. Figure 4 also displays the linear-drag model computed from Eq. 2 (dashed line). The measured ΔE_i of the DD-t and D^3He-α were used to determine $\ln\Lambda_{exp}$ from the linear drag model (Eqs. (2) and (4)). This was done for every shot shown in Table I. Since $\mathcal{C}$ is expected to be constant at these plasma conditions, $\mathcal{C}$ is fit to all measurements of $\ln\Lambda_{exp}$, where $\langle n_e \rangle$ and $\langle T_e \rangle$ were used to calculate λ_{De} and λ_Q. The result is shown in Figure 5. The best fit yields $\mathcal{C} = 0.43 \pm 0.12$, which minimizes $\ln\Lambda_{exp} - \ln(\mathcal{C}\lambda_{De}/\lambda_Q)$. This result is consistent with the qLB, qFP, and BPS predictions, indicating that the small angle scattering is well described by the first-Born approximation of the elastic scattering cross section. The measurements are inconsistent with the 'GMS6' model, which is a fit to T-matrix calculations over a wide parameter space. Subsequently, our data implies the fitted formulas for the T-matrix results should be revisited for accuracy.

In summary, the first high-precision measurements of i-e energy-transfer cross section in a weakly-coupled and non-degenerate HED plasma were conducted using a novel technique based on low-velocity ion-stopping-power measurements. The measurements determined the Coulomb logarithm and showed that i-e energy transfer in this regime is well described by qLB, qFP, or BPS theories. The applicability of these theories extends further than the scope of the measurements, as they are expected to be accurate for non-degenerate ($\Theta \gg 1$), weakly coupled ($\Gamma \ll 0.1$) plasmas where $\lambda_L/\lambda_Q \ll 1$. Our results are relevant to the energy balance in ICF hot spots ($n_e \sim 10^{24} - 10^{26}/cm^3$ and $T_e \sim$ 3-5 keV) and laser ablation ($n_e < 10^{21}/cm^3$ and $T_e \sim$ 1-3 keV), as well as astrophysical systems such as supernovae shocks ($n_e < 1/cm^3$ and $T_e > 0.1$ keV). Simulations that model plasmas in these regimes should implement the i-e energy transfer cross section of qLB, qFP, or BPS to provide the most accurate ion-electron energy transport. In future experiments, the low-velocity ion stopping technique will be leveraged to probe ion-electron energy exchange in more degenerate and strongly coupled plasmas where the qLB, qFP, and BPS model begin to disagree, as shown in Fig 1.

ACKNOWLEDGMENTS

This work was supported by the U.S. Department of Energy under Grant No. DE-NA0003868, the Laboratory for Laser Energetics under Grant No. 417532G/UR FAO GR510907, Lawrence Livermore National Laboratory under Contract DE-AC52-07NA27344, and the National Laser Users Facility under Grant No. DE-NA0003938. P.J.A. was supported under Grant No. DE-NA0003960. R. F. was supported under Grants No. GOB-ESP2019-13 (ULPGC) and PID2019-108764RB-I00 (MICNN, Spain).

[1] Y. B. Zel'dovich and Y. P. Raizer, *Physics of Shock Waves and High-Temperature Hydrodynamic Phenomena*, Academic Press, 1967.

[2] S. Atzeni and J. Meyer-ter Vehn, *The physics of inertial fusion: beam plasma interaction, hydrodynamics, hot dense matter*, Oxdord University Press, 2004.

[3] M. J.-E. Manuel et al., Physics of Plasmas **20**, 056301 (2013).

[4] M. J.-E. Manuel et al., Physics of Plasmas **22**, 056305 (2015).

[5] C.-K. Li and R. D. Petrasso, Physical Review Letters **70**, 3063 (1993).

[6] H. Brysk, P. M. Campbell, and P. Hammerling, Plasma Physics **17**, 473 (1975).

[7] A. B. Zylstra and O. A. Hurricane, Physics of Plasmas **26**, 062701 (2019).

[8] P. Ghavamian, S. J. Schwartz, J. Mitchell, A. Masters, and J. M. Laming, Space Science Reviews **178**, 633 (2013).

[9] M. van Adelsberg, K. Heng, R. McCray, and J. C. Raymond, The Astrophysical Journal **689**, 1089 (2008).

[10] J. Vink, S. Broersen, A. Bykov, and S. Gabici, Astronomy & Astrophysics **579**, A13 (2015).

[11] L. D. Landau, Zh. Eksp. Teor. Fiz. **7** (1937).

[12] L. Spitzer Jr., *Physics of Fully Ionized Gases, 2nd ed.*, Wiley Interscience, 1962.

[13] M. W. C. Dharma-Wardana and F. Perrot, Physical Review E **58**, 3705 (1998).

[14] D. O. Gericke, M. S. Murillo, and M. Schlanges, Physical Review E **65**, 036418 (2002).

[15] D. O. Gericke, Journal of Physics: Conference Series **11**, 111 (2005).

[16] L. S. Brown, D. L. Preston, and R. L. Singleton Jr., Physics Reports **410**, 237 (2005).

[17] L. S. Brown and R. L. Singleton, Physical Review E **76**, 066404 (2007).

[18] G. Dimonte and J. Daligault, Physical Review Letters **101**, 135001 (2008).

[19] G. Gregori and D. O. Gericke, Euro-physics Letters **83**, 15002 (2008).

[20] J. N. Glosli et al., Physical Review E **78**, 025401(R) (2008).

[21] B. Jeon et al., Physical Review E **78**, 036403 (2008).

[22] J. Daligault and G. Dimonte, Physical Review E **79**, 056403 (2009).

[23] J. Vorberger and D. O. Gericke, Physics of Plasmas **16**, 082702 (2009).

[24] F. R. Graziani et al., High Energy Density Physics **8**, 105 (2012).

[25] L. X. Benedict et al., Physical Review E **86**, 046406 (2012).

[26] D. A. Chapman, J. Vorberger, and D. O. Gericke, Physical Review E **88**, 013102 (2013).

[27] F. Graziani, M. P. Desjarlais, R. Redmer, and S. B. Trickey, editors, *Frontiers and Challenges in Warm Dense Matter*, Lecture Notes in Computational Science and Engineering, Springer International Publishing, 2014.

[28] J. Daligault, Physics of Plasmas **23**, 032706 (2016).

[29] L. G. Stanton and M. S. Murillo, Physical Review E **93**, 043203 (2016).

[30] L. X. Benedict et al., Physical Review E **95**, 043202 (2017).

[31] C. R. Scullard, S. Serna, L. X. Benedict, C. L. Ellison, and F. R. Graziani, Physical Review E **97**, 013205 (2018).

[32] S. Rightley and S. D. Baalrud, Physical Review E **103**, 063206 (2021).

[33] J. A. Gaffney et al., Physics of Plasmas **26**, 082704 (2019)

[34] J. R. Rygg et al., Physical Review E **80**, 026403 (2009).

[35] C. L. Ellison et al., Physics of Plasmas **25**, 072710 (2018).

[36] M. Gatu Johnson et al., Physics of Plasmas **25**, 056303 (2018).

[37] H. D. Whitley et al., High Energy Density Physics **38**, 100928 (2021).

[38] T. Kihara and O. Aono, Journal of the Physical Society of Japan **18**, 837 (1963).

[39] D. Gerkie, Laser and Particle Beams **20**, 471474 (2002).

[40] D. O. Gericke, M. Schlanges, and T. Bornath, Physical Review E **65**, 036406 (2002).

[41] D. J. Bernstein, S. D. Baalrud, and J. Daligault, Physics of Plasmas **26**, 082705 (2019).

[42] J. Frenje et al., Physical Review Letters **115**, 205001 (2015).

[43] J. Frenje et al., Physical Review Letters **122**, 015002 (2019).

[44] T. R. Boehly et al., Optics Communications **133**, 495 (1997).

[45] C. Stoeckl et al., Physical Review Letters **90**, 235002 (2003).

[46] D. G. Hicks et al., Physics of Plasmas **7**, 5106 (2000).

[47] F. H. Sguin et al., Review of Scientific Instruments **74**, 975 (2003).

[48] L. Ballabio, J. Kllne, and G. Gorini, Nuclear Fusion **38**, 1723 (1998).

[49] H. Sio et al., Review of Scientific Instruments **87**, 11D701 (2016).

[50] R. Florido et al., Physical Review E **83**, 066408 (2011).

[51] R. Florido et al., Physics of Plasmas **21**, 102709 (2014).

[52] T. Nagayama et al., Physics of Plasmas **21**, 050702 (2014).

[53] J. T. Larsen and S. M. Lane, Journal of Quantitative Spectroscopy and Radiative Transfer **51**, 179 (1994).

[54] F. H. Sguin et al., Review of Scientific Instruments **75**, 3520 (2004).

[55] V. Y. Glebov et al., Review of Scientific Instruments **75**, 35593562 (2004).

[56] B. Xu and S. X. Hu, Physical Review E **84**, 016408

(2011).
[57] S. D. Bergeson et al., Physics of Plasmas **26**, 100501 (2019);
[58] G. Maynard and C. Deutsch, Physical Review A **26**, 665 (1982).
[59] G. Zimmerman, LLNL Report No. UCRL-JC-105616 (1990).
[60] M. R. Zaghloul et al., Physics Letters A **268** 375-381 (2000).
[61] Here it is assumed the ion-ion stopping power is negligible compared to the ion-electron stopping power. This is valid if $V_i >> V_{Thi}$, where V_{Thi} is the ion thermal velocity.
[62] The energy loss of the DD-t is in agreement with the BPS theory, which was not the case reported in previous work [43]. The DD-t energy loss was reconciled with theory by accounting for the fact that the energy loss explicitly depends on Z_i^2/m_i of the ion (see Supplemental Material) and that the DD-t energy loss has a small ion-ion component.
[63] Measured with the PXTD diagnostic [49]. Absolute error is $\pm 50ps$
[64] Absolute Yield errors are 5% of measured value.
[65] Absolute error $\pm 20keV$.
[66] $\langle T_i \rangle$ inferred from DD-neutron spectrum [55].
[67] $\langle n_e \rangle$,$\langle n_e L \rangle$, and $\langle T_e \rangle$ are the dE/dx-weighted plasma conditions probed by the fusion products. See Supplemental Material.
[68] Shots 78611 and 78612 did not measure DD-t particles and only the D3He-α was used to infer $\ln\Lambda_{exp}$.
[69] Pulse shape 1 ns square.